Polymer Bulletin (2025) 82:4577–4603
https://doi.org/10.1007/s00289-025-05733-3

ORIGINAL PAPER

RSM and ANN modeling-based optimization approach for the development of alginate-chitosan particles containing *Rosmarinus officinalis* essential oil

Lamia Taouzinet[1] · Sofiane Fatmi[2,3,4] · Amina Kribeche[5,6] · Mohamed Skiba[4] · Mokrane Iguer-Ouada[2]

Received: 16 April 2024 / Revised: 26 December 2024 / Accepted: 9 March 2025 /
Published online: 22 March 2025

Abstract

Alginate is a multifunctional biopolymer employed in diverse applications, particularly in delivery systems that safeguard bioactives in acidic environments. Chitosan demonstrates various functionalities, including enhanced mucoadhesion and the facilitation of controlled release in alkaline conditions. Current research focuses on encapsulating essential oils in alginate and chitosan. The study aimed to encapsulate *Rosmarinus officinalis* essential oil within the alginate-chitosan sphere to enhance its physical properties and investigate the protective effects of alginate-chitosan *Rosmarinus* essential oil particles during sperm cryopreservation. The effects of factors influencing cell motility were optimized and modeled using response surface methodology and artificial neural networks. Results indicated a high goodness of fit for the artificial neural network model with an R^2 of 0.999, compared to 0.991 for the response surface methodology. The optimal solution involved 2 g of alginate, 1.05 g of chitosan, and 80 µl of *Rosmarinus* essential oil. The optimal formulation was characterized by assessing drug entrapment efficiency, drug-excipient interaction, swelling index, and lipid peroxidation state. At pH 6.8, alginate-chitosan-*Rosmarinus* essential oil particles exhibited a significant swelling index. These findings suggest that the formation of alginate-chitosan through cross-linking holds promise for solubilizing and delivering *Rosmarinus* essential oil to sperm under cryopreservation conditions. Adding alginate-chitosan-*Rosmarinus* essential oil complex to the extender enhances its ability to remove free radicals and thus protects sperm during the cryopreservation process. A methodological approach utilizing either response surface methodology or artificial neural networks can establish alginate-chitosan encapsulation effectively. Importantly, the artificial neural network model outperformed response surface methodology in prediction and optimization accuracy.

Keywords Sodium alginate · Chitosan · *Rosmarinus officinalis* essential oil · Response surface methodology · Artificial neural network

Extended author information available on the last page of the article

Introduction

Drug encapsulation represents a pivotal research avenue for the development of modern pharmaceutical forms. It serves to tackle various challenges, including susceptibility to oxidation, volatility, incompatibility, poor absorption, and rapid release during the manufacturing process [1]. Encapsulation vitrification has been successfully used for the long-term preservation of testis tissue [2, 3] and cells such as spermatogonial stem cells [4–6]. A multitude of encapsulation systems are available, including liposomes [7, 8], cyclodextrins [9], and polyethylene glycol [10]. Microencapsulation technologies and methods involving liquid or gas solidification play a key role in mitigating the loss of volatile core materials, isolating and safeguarding active ingredients, enhancing core material stability, and enabling precise control over its release kinetics [11]. Numerous studies have highlighted the encapsulating potential of alginate (Alg) and chitosan (Chi) due to their mucoadhesive [12], biodegradable [13], and non-toxic properties [14].

Chitosan is a positively charged polysaccharide that occurs naturally. It is derived by deacetylating a segment of chitin molecule [15]. The molecular chain of Chi consists of structural units of N-glucan and N-acetyl-glucan [16]. The chemical properties of chitosan reveal its insolubility in water, attributed to the absence of protonation under neutral and alkaline pH conditions [17, 18]. The permeation mechanism relies on the positive charges of Chi; these charges can improve the permeation properties and induce structural rearrangement, leading to the association of tight junction proteins [19]. Given its outstanding biocompatibility, degradability, non-mammalian origin, antibacterial properties, cationic characteristics for interacting with anionic drugs, ability to cross-link, control over swelling, and the high degree of deacetylation, Chi proves to be highly suitable for use in delivery systems [20, 21]. As an encapsulating material, Chi is vulnerable to acidic environments, which could lead to a rapid release of encapsulated substances in the stomach. On the other hand, Chi has been reported to be used in sperm cryopreservation [22]. Therefore, combining Chi with other encapsulated substances using electrostatic interactions, hydrogen bonding effects, hydrophobic interactions, and similar mechanisms will address this scientific challenge. The advancement of intelligent delivery systems has garnered significant interest in alginate [23].

Alginate as an anionic polymer has been extensively studied as a physically cross-linked polymer. It forms a gel at room temperature and physiological pH levels because of ionic interactions [24]. It can be easily processed in hydrophilic solvents, demonstrating outstanding biocompatibility, controllable degradation, self-healing properties, and reported non-toxicity [25]. The inherent characteristics of pure Alg include poor viscoelasticity and high permeability. To enhance its physicochemical properties, researchers commonly employ a composite approach, combining Alg with various natural or synthetic polymers. It readily forms a polyelectrolyte complex with polycations such as Chi, exhibiting synergistic effects in chemical, rheological, and mechanical properties, as reported in the studies [26, 27]. However, at higher pH levels, it transforms into a soluble

viscous layer, releasing materials [28, 29]. In recent times, it has been utilized as a framework for tissue regeneration within the realm of regenerative medicine. Additionally, alginate oligosaccharide is described as a biodegradable polymer possessing attributes such as antioxidant, anti-inflammatory, anti-apoptotic, and anti-proliferative effects, all the while being non-allergenic and non-toxic [30]. Consequently, they find extensive application as conveyors for delivering drugs, in immunoisolation systems for transplantation, as dressings for wounds, and as protective agents in radiotherapy [31, 32]. In a similar context, Kumar et al. (2019) demonstrated that adding sodium alginate to buffalo semen extender enhanced antioxidant capacity, free radical scavenging, and metal reduction capability while preserving sperm during cryopreservation [33]. Alginate is used as cryopreservation medium for cell encapsulation to prevent premature acrosome reactions and protect sperm DNA from denaturation during rapid freezing [34].

Current research endeavors predominantly concentrate on encapsulating volatile oils using composite wall materials. This approach aims to achieve controlled and sustained drug release while preserving the properties of volatile oils [35]. Essential oils are aromatic, volatile liquids extracted from plants and renowned for their therapeutic properties. They find extensive applications as flavoring agents in food, fragrances in perfumes, and ingredients in pharmaceutical products [36]. Among the many essential oils, the essential oil of *Rosmarinus officinalis* (Rom) is known for its high therapeutic potential. Rom, in particular, is a highly concentrated hydrophobic liquid containing volatile aromatic compounds derived from the plant [37]. This oil contains diverse chemical compounds, including monoterpenes like 1,8-cineol, borneol, pinene, limonene, camphene, camphor, and myrcene [38]. *Rosmarinus officinalis* is utilized to treat affections ranging from mild forms of dyspepsia and spasmodic gastrointestinal disorders to circulatory issues. It is also recognized for its complementary benefits in addressing muscle or joint pain and inflammation [39]. Moreover, reports have suggested that Rom can enhance sperm mobility and viability [40]. Recent applications of Rom include its use *in ovo* injection [41]. However, Rom exhibits poor physical properties like hydrophobicity, susceptibility to degradation, and volatility, rendering them challenging for use in pharmaceutical and food applications [42]. These drawbacks can be partially overcome by encapsulating these essential oils in the Alg-Chi complex [18]. To the author's knowledge, no related studies have been conducted yet on the formulation of Alg-Chi-Rom particles as a supplement in sperm cryopreservation medium.

Considering that traditional one-factor-at-a-time formulation studies are time-consuming and costly, it is preferable to utilize alternative methods such as response surface methodology (RSM) and artificial neural networks (ANN) to optimize Rom encapsulation in Alg-Chi complex conditions [43]. Response surface methodology (RSM) is a widely accepted mathematical and statistical approach used to construct experimental models. It helps to assess the relative significance of each independent variable and to identify the optimal operational conditions necessary to achieve the desired outcomes. The RSM is a valuable tool for studying interactions among multiple variables and has been effectively used to optimize parameters in various processes [44–47]. Inspired by the biological nervous system, the artificial neural network (ANN) approach can be employed to model the process and identify the

most influential variables [43]. In contrast, the artificial neural networks (ANN) method has emerged as an alternative to RSM for simulating complex technological processes. The ANN method can establish nonlinear connections between independent and dependent variables without requiring prior knowledge of the relationships between intended responses [48]. Compared to other data acquisition techniques like RSM, ANN stands out as a powerful tool. It offers enhanced accuracy and efficiency by flexibly modeling experimental data, predicting outcomes, and modeling biochemical processes [49]. The state of the art did not find any studies on formulating Alg-Chi-Rom using an experimental design and artificial neural network approaches, particularly for demonstrating their performance in cryopreserved sperm motility studies.

Therefore, in this study, we encapsulated Rom in the Alg-Chi sphere to improve its physical properties and explore how Alg-Chi-Rom particles can protect sperm during cryopreservation. Thus, the effects of factors affecting cell motility were optimized and modeled using the RSM and ANN methods. The optimal Alg-Chi-Rom formulation is characterized by assessing drug entrapment efficiency, drug-excipient interaction, swelling index, and lipid peroxidation state.

Experimental section

Materials

Chitosan (Low molecular weight; Assay deacetylation: $\geq 75\%$; Viscosity (1% in 1% Acetic Acid): 20–300 cps); Sodium alginate (Solubility (Turbidity) (100 mg plus 10 ml of water): Slightly Hazy to Very Hazy; Brookfield Viscosity (2% in water at 25°): >2000 cps) HPLC-grade solvents and *Tris* buffer were purchased from Sigma-Aldrich, USA. The other entire reagent used was of analytical grade.

Methods

Experimental design

The experimental design offers a powerful means to concurrently evaluate multiple factors and eliminates the need for an exhaustive number of individual runs typically required in a traditional step-by-step approach. This study used a systematic optimization method in which the aim was to improve sperm motility, which was the key factor to be closely examined. The Box–Behnken design was harnessed to conduct a statistically rigorous optimization of the formulation parameters. This design facilitated a comprehensive assessment of the key factors, their interactions, and quadratic effects on sperm motility. The choice of a 3-factor, 3-level design allowed the exploration of quadratic response surfaces and the development of second-order polynomial models. Notably, this cubic design features points located 9 at the midpoint of each edge within a multidimensional cube, along with central point replicates

($n=3$), a design aspect that conveniently avoids extreme factor combinations. By mitigating the risk of data loss, this design ensures robust and reliable results.

A design matrix comprising 15 experimental runs was meticulously constructed, paving the way for the formulation of a nonlinear computer-generated quadratic model (Eq. (1)). This model served as a valuable tool to comprehensively analyze the interplay of factors, predict responses, and optimize the Alg-Chi-Rom formulation.

$$Y = \beta 0 + \sum_{i=1}^{3} \beta i\, Xi + \sum_{i=1}^{3} \beta ii\, Xi^2 + \sum_{i=1}^{2} \sum_{j=i+1}^{3} \beta ij\, Xi\, Xj \tag{1}$$

where Y is the measured response associated with each factor level combination;$\beta 0$ is a constant; βi, βii, and βij are the constant coefficients; Xi and Xj are the coded independent variables.

To increase the radius from the center of the original design, the option of ridge max was employed to compute the estimated ridge of maximum response. In this study, we used the independent variables' real values to assure that the model coefficients could be directly interpreted according to the actual experimental settings. The independent variables examined were the amount of the bio-adhesive polymers: Alg (X1), Chi (X2), and the volume of Rom (X3). The dependent variable was sperm motility (Y). The concentration range of the independent variables under study, along with their low, medium, and high levels, are shown in Table 1. Optimizing the concentrations of chitosan and alginate in both cell preservation media and encapsulation is a crucial procedure for guaranteeing the stability and viability of cells or encapsulated substances. Therefore, we have chosen an interval that encompasses both application domains (X_1 and X) [50–54]. The range of Chi values has been limited to 0.1 and 2 (% w/v) due to the observed consequences outside of this range. When Chi and Alg lack bonds, the mechanical resilience of the particles rises with an escalation in Chi cross-linking, indicating that highly cross-linked particles would exhibit reduced swelling. Consequently, this leads to decreased penetration of internal water and the diffusion of external drugs. Similarly, controlling the degree of deacetylation and molecular mass can control the drug release profile. Moreover, understanding the nature of the properties and optimizing them may result in better drug formulations with sustained release rates [18, 23, 55]. Regarding the rosemary

Table 1 The concentration range of independent variables

Factor	Levels used, actual (coded)		
	Low (− 1)	Medium (0)	High (+ 1)
X1 = Sodium alginate (% w/v)	1	2	3
X2 = Chitosan (% w/v)	0.10	1.05	2
X3 = Rom (µl)	10	80	150
Dependent variables	Constraints		
Y = sperm motility (um/s)	Maximize		

essential oil concentration, Benberkan et al. (2019) conducted an optimization study to determine its ideal concentration for sperm cryopreservation (X_3) [40].

Artificial neural network (ANN)

The multilayer full feed-forward (MFFF) was applied in the ANN modeling for the study of sodium alginate-chitosan particles containing Rosmarinus officinalis essential oil. The established ANN models comprised an input layer, a hidden layer, and an output layer [56]. In this study, two hidden layers have been chosen as it is efficient for the large majority of problems; otherwise, more hidden layers may result in an overfitting problem. For this, the study was scheduled using a less complex model [57]. The input layer of the proposed ANN model had three nodes (neurons), which represented the factors mentioned earlier in the experimental design, namely the amount of the bio-adhesive polymers: Chi, Alg, and the volume of Rom. The output layer had one neuron, which represented sperm motility. In this ANN model, the number of hidden neurons in the hidden layer, the learning algorithms, the nonlinear transfer functions for the hidden layer and output layer, and the repetitions were optimally determined. The iteration number was chosen as 1000, and the optimum neural network configuration was obtained as 3-3-7-1. The early stopping approach was used to deal with any overfitting problem [57]. Furthermore, the learning algorithm employed 75% of the experimental data as a training set and 25% as a validating set. The ANN model architecture is illustrated in Fig. 1. Therefore, the best ANN model was finally established.

Additionally, a single output (Y) is produced by each of the several artificial neurons that make up the artificial neural network (ANN) from all of the inputs (Xi) using a straightforward Eq. (2) that can be graphically understood.

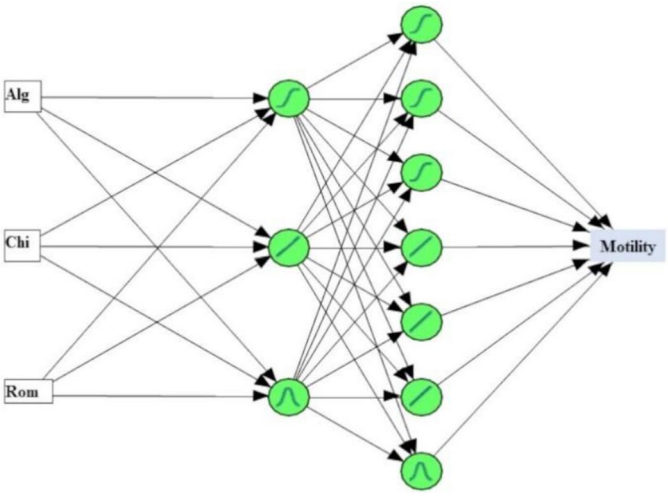

Fig. 1 The ANN model architecture

$$Y = f(H) = 1/1 + e^{-H} \tag{2}$$

f is the activation function. However, H is the weighted total of the inputs plus a bias coefficient indicated by (b) that regulates the impact of the function (Eq. (3)).

$$H = \sum_{i=1}^{n} x_i w_i + b \tag{3}$$

Preparation of *Rosmarinus officinalis* essential oil particles

Chitosan solutions at three different concentrations (0.1%, 1.05%, and 2% w/v) were prepared by dissolving Chi in a 1% acetic acid solution and adding 4% calcium chloride. The resulting solution was subjected to homogenization at 500 r.p.m. for 1 h. The sodium alginate solution was prepared with 1%, 2%, and 3% (w/v). After mixing sodium alginate, Rom was incorporated at a concentration of 0.2% (w/v). The sodium alginate-drug solution was delivered into the chitosan-calcium chloride solution via a syringe needle at a controlled drop rate of 1.0 ml/min. The microparticles were left to harden for 2 h, followed by thorough washing and drying at room temperature (Fig. 2).

Epididymal semen collection

Bovine testes were obtained from a local slaughterhouse and transported to the laboratory under cold conditions. Sperm collection was conducted using the retrograde flushing method previously described by Martinez-Pastor et al. (2006). In brief, the

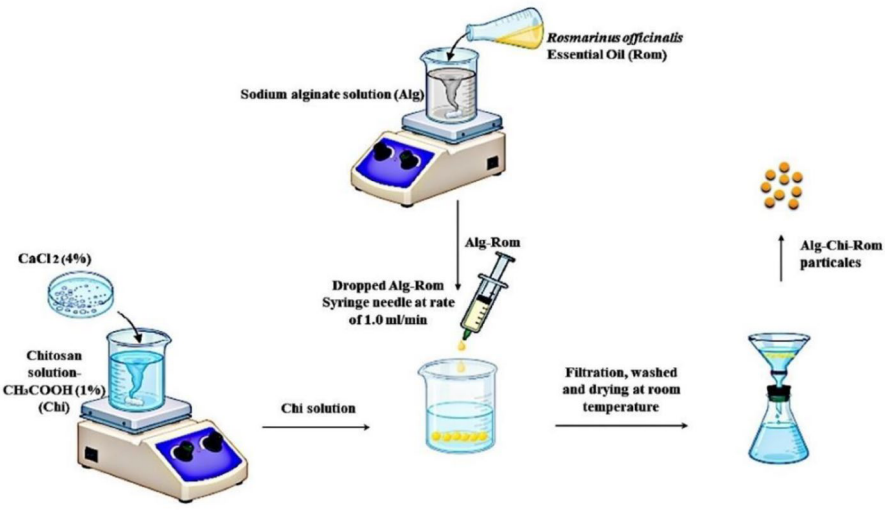

Fig. 2 Preparation of Alg-Chi-Rom

epididymis was separated from the testes and carefully cleaned. Both the cauda and vas deferens were isolated from the entire epididymis. Blood vessels in the cauda epididymis were severed, and the cauda's surface area was thoroughly rinsed and wiped clean. Sperm retrieval was accomplished by applying pressure from the vas deferens, manually generated using a syringe containing air and a 1 ml extender. Sperm was released from a cut made in the distal cauda, near its junction with the corpus [58].

Semen dilution, cold preservation, and motility analysis

For analysis, 5 µl of each sperm sample was placed in a Makler® chamber (Sefi Medical Instrument) previously equilibrated to 37 °C and examined using a phase-contrast microscope (Nikon E200®-LED microscope, Japan). A Tris-based extender was employed in this study, consisting of 30.8 g/l Tris, 17 g/l citric acid, and 12.5 g/l fructose.

The treatment solutions were prepared by adding Rom at a concentration of 0.8 µl/ml and the optimal Alg-Chi-Rom solution, with the same concentration as the non-encapsulated Rom, to the Tris-based extender. Sperm motility parameters were assessed using a computer-assisted sperm analyzer (CASA) (Sperm class analyzer, SCA Microptic, S.L., Version 3.2.0, Barcelona, Spain). To ensure optimal image capture and prevent spermatozoa cell overlap, sperm samples were appropriately diluted to maintain a concentration below 40×10^6 spermatozoa (Spz)/ml. Images were captured using a video camera (Digital Camera Basler A312fc, Germany) at a magnification of × 10 (negative phase contrast). The sperm motility parameters assessed by CASA included total motility (%), progressive motility (%), curvilinear velocity (VCL µm/s), straight linear velocity (VSL µm/s), and average path velocity (VAP µm/s) [7].

Characterization of the optimal Alg-Chi-Rom

High-performance liquid chromatography (HPLC) analysis To confirm the presence of *Rosmarinus officinalis* in Alg-Chi spheres, camphor, an active compound found in Rom, was used as an indicator.

Samples of pure Rom, chitosan, sodium alginate, Alg-Chi-Rom, and camphor were individually dissolved in methanol under sonication. After sonication, the samples were filtered. Camphor was quantified at 370 nm using an HPLC system, comprising LPG 3400 pumps, an ACC 3000 autosampler, and VWD 3400 RS variable wavelength detectors. Chromatographic separation was achieved using a C-18 column (150 × 4.6 mm, 5 µm). The mobile phase was a mixture of water and acetonitrile in a 3:2 ratio, with an isocratic flow rate of 1.5 ml/min.

Determination of drug entrapment efficiency (DEE) The Rom content was assessed by dissolving 100 mg of microparticles in a phosphate buffer with a pH of 7.4. This dissolution process was facilitated by sonication for 30 min, ensuring the complete dissolution of the microparticles. The resulting solutions were then filtered and sub-

jected to HPLC analysis. To calculate the encapsulation efficiency, the following formula was applied:

$$\text{Drug entrapment efficiency (\%)} = (\text{calculated drug concentration/theoretical drug concentration}) * 100$$

Drug-excipient interaction study by Fourier transform infrared spectroscopy Fourier transform infrared spectrum of pure Rom, chitosan, sodium alginate, alginate-chitosan physical mixture, and Rom microsphere was recorded in the range of 4000–400 cm^1 using FT–IR (Perkin Elmer) from the KBr pellet to find out the drug-excipient compatibility study.

Swelling index study A swelling study for the sphere was conducted by immersing the sphere in 50 ml of three respective media, namely, simulated gastric fluid pH 1.2 and simulated intestinal fluid phosphate buffer pH 6.8 and pH 7.4. The increase in weight of the sphere was determined at preset time intervals until a constant weight was observed by using the Mettler Toledo single-pan electronic balance. The swelling index was then calculated as.

$$\text{Swellingindex} = (\text{Mass of swollen spheres—Mass of dry spheres} / \text{Mass of dried spheres}) * 100$$

Thiobarbituric acid reaction substances (TBARs) assay The samples for the TBARs assay were prepared as described by [59]. Briefly, the spermatozoa from four straws (1000 µl containing 100×10^6 Spz) of each treatment were centrifuged at 1500 ×g for 15 min, and the supernatant was eliminated. The sperm was washed by resuspending twice in 1 ml of distilled water and centrifuging (1500 ×g for 10 min). The supernatant from the last centrifugation was discarded, and the pellet was resuspended in 500 µl of distilled water and sonicated for 15 s on ice. The procedure was repeated six times at intervals of 30 s. The sonicated sperm was used for lipid peroxidation measurement by the TBARS assay. The TBARs assay is based on the measurement of malondialdehyde (MDA). MDA, the final product of the lipid peroxidation chain reaction, was quantified by thiobarbituric acid (TBA) as described by [60]. Briefly, 1 ml of TTH solution (trichloracetic acid 15%, w/v, thiobarbituric acid 0.375%, w/v in hydrochloric acid 0.25 N) was added to sonicated spermatozoa (0.5 ml). The mixture was incubated at 95 °C in a boiling water bath for 60 min to induce the MDA-TBA reaction. After cooling with ice water, the tubes were centrifuged at $18{,}000 \times g$ for 15 min. The supernatant was then recovered, and the malondialdehyde (MDA) was estimated by spectrophotometry at 532 nm. The molar extinction coefficient for MDA is 1.56×10^5/M cm. The results were expressed as nmol MDA/10^8 Spz.

Table 2 Observed and predicted responses using BBD and ANN models for Alg-Chi-Rom

Test	Configuration	Alg	Chi	Rom	Mobility	RSM predicted motility	ANN-predicted Motility
1	+−0	3	0.1	80	27.76	26.42	27.70
2	+0+	3	1.05	150	28.27	27.04	28.32
3	0−−	2	0.1	10	21.04	21.04	21.09
4	000	2	1.05	80	24.98	24.84	24.73
5	000	2	1.05	80	25.02	24.84	24.73
6	−0+	1	1.05	150	20.87	29.53	20.96
7	−−0	1	0.1	80	33.86	32.63	34.01
8	000	3	2	80	9	10.23	9.09
9	0−+	2	0.1	150	65.4	67.97	48.13
10	++0	2	1.05	80	24.52	24.84	24.73
11	0++	2	2	150	18.36	18.36	22.68
12	0+−	2	2	10	30.83	38.26	30.82
13	−0−	1	1.05	10	18.51	19.74	18.37
14	−+0	1	2	80	15.09	16.43	11.18
15	+0−	3	1.05	10	8.48	9.82	8.39

Table 3 Analysis of variance for the Alg-Chi-Rom formulation on sperm motility

	Source	Coefficient	DF	SS	SM	*p* value	Prob > F
Motility	Model		9	2485.21	276.13	0.0002	> 0.0002
	Residual		5	23.45	4.69		
	Lack of fit		3	23.29	7.76		
	Pure error		2	0.15	0.08		
	Corrected total		14	2508.65			
	R	0.991					
	Adj-	0.974					
	CV* (%)	33.616					
	RMSE**	2.165					
	MSE***	4.687					
	MAE****	1.333					
	MAPE****	0.358					

*Coefficient of variation, **Root mean squared error, ***Mean squared error, ****Mean absolute error, ****Mean absolute percentage error

Results and discussion

Alg-Chi-Rom modeling and optimization

The influence of Alg-Chi-Rom formulation on sperm motility using the

Table 4 Estimation parameters of the ANN model for training and validation data

Motility		
	Training	Validation
R^2	0.999	0.995
RMSE*	0.209	1.382
Log-likelihood	− 1.561	6.969
SSE**	0.485	7.638
MAE***	1.14	
MAPE****	0.306%	

*Root mean squared error, **Sum of squared errors, ***Mean absolute error, ****Mean absolute percentage error

Box–Behnken design and ANN model is exposed in Table 2**.**

The data clearly indicate a remarkable similarity between the predicted and observed values for the Alg-Chi-Rom formulation, as evidenced by the experimental data. This alignment in the results can be further supported through regression analysis, as shown in Table 3 for the RSM model and Table 4 for the ANN model.

A well-fitted model should have an R^2 value of at least 0.80. The sperm motility R^2 values in this study were 0.991 for the RSM model (Table 3), suggesting a strong fit and prediction model. This means that 99% of the variability in sperm motility can be attributed to the independent parameters, and only 1% was not explained by the model. As a result, it is advisable to use an adj-R^2 to assess the model's appropriateness [61]. Table 3 shows that the sperm motility model's R^2 and adj-R^2 values are not statistically different, indicating that non-significant factors were not included in the model. The root mean squared error (RMSE) was 2.16. This indicates that the estimated model matches the experimental data adequately. The CV value was found to be 33.616%. The CV is a statistical tool that reflects the standard deviation as a proportion of the mean; lower values of the CV give higher repeatability. In general, a CV larger than 10 indicates that the mean value exhibits considerable variations and that an appropriate response model has not been effectively created [62]. It follows that sperm motility varies greatly from one to the next. The regression model equation provides an excellent fit to the experimental data and makes a plausible prediction, as seen by the low pure error values observed in model terms (Table 3).

The data were analyzed statistically using Analysis of Variance (ANOVA) to evaluate the importance of the main effects and interactions of the specified factors on sperm motility. Multiple linear regressions were then used to develop the polynomial factorial equation for predicting sperm motility. The resulting equation is as follows:

$$\begin{aligned}\textbf{Motility sperm} = {} & 24.84 - 1.85\ \text{Alg} - 9.35\ \text{Chi} - 6.75\ \text{Rom} - 9.14\ \text{Alg}^2 + 5.73\ \text{Chi}^2 \\ & + 3.33\ \text{Rom}^2 + 0.0025\ \text{Alg.Chi} + 4.35\ \text{Alg.Rom} - 14.21\ \text{Chi.Rom}\end{aligned} \tag{4}$$

Equation (4) describes the link between sperm motility, the three variables (Alg, Chi, and Rom), and their interactions. The ANOVA findings showed that these factors had a significant effect on sperm motility, as seen by the wide range of coefficients in the equation. The coefficients β_2, β_3,β_{11},β_{22} , β_{33},β_{13}, and β_{23} were found to be significant at $P < 0.05$, while the significance level of coefficients β_1 and β_{12} was found to be greater than 0.05. Thus, interaction terms β_1 and β_{12} do not contribute significantly to the prediction of sperm motility. The results revealed that increasing X_1, X_2, and X_3 values induce a decrease in sperm motility. In summary, it was found that sperm motility depends on the Alg-Chi-Rom composition.

The positive and negative values indicate the impacts of Alg, Chi, and Rom amounts. The fact that the results of Alg, Chi, Rom, Alg^2, and Chi. Rom are negative indicates that these terms influence sperm motility negatively. The coefficients of Eq. (4) indicated that the positive influence of the individual formulation parameters on sperm motility was ranked first by the Chi, followed by the Rom. This result can be explained by the fact that Chi exhibits higher viscosities at lower temperatures due to increased molecular interactions and reduced molecular mobility [63–65]. As the concentration of chitosan increased, the average particle size exhibited a relatively higher value compared to other formulations. This phenomenon is attributed to the elevated concentrations of chitosan/alginate. Increased polymer concentrations have been observed to correlate with larger particles, as demonstrated by Guinebretière et al. (2002) [55]. It is conceivable that the electrostatic interactions between chitosan and alginate play a role in bolstering particle stability and size [18]. Concurrently, the sluggish solubility of sodium alginate in cold water results in the formation of a viscous solution [66]. Furthermore, the significant amount of Alg and Chi exerts a negative influence on particle rigidity, potentially impacting the delivery of drugs or active compounds [67]. These factors contribute to challenges in sperm motility within the aqueous

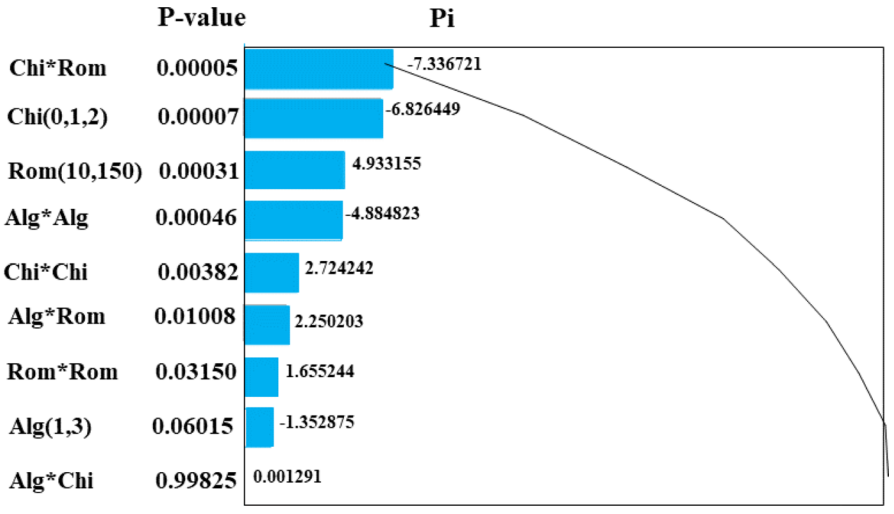

Fig. 3 A. Pareto analysis and variable effect graphic

environment, resulting in reduced mobility. The influence of Rom shows a negative effect on sperm motility, as evident in Eq. (4) and Fig. 3, with a positive coefficient for Rom.Rom. It is essential to note that the use of moderate Rom dosages is crucial because an excessive dose can have a spermicidal effect. Previous research by Benberkane et al. (2019) has indicated that low doses of Rom offer protection against cryopreservation damage [40]. However, chitosan, which is an oligosaccharide molecule [68], can act as a cryoprotective agent and can be used to enhance the delivery of hydrophobic drugs. This benefit is reflected in a positive effect (Chi.Chi) on sperm motility.

The Pareto analysis provides essential information for interpreting these results [69]. This study determines the percentage effect of each variable on the response based on the relationship Eq. (5).

$$\boldsymbol{P}_i = \frac{\mathrm{bi}^2}{\sum \mathrm{bi}} \times 100(i \neq 0) \tag{5}$$

where *bi* represents the estimation of the principal effect of factor *i* on the response.

Figure 3 depicts the same findings obtained in the polynomial equation as the impact of the examined variables and their interactions on sperm motility.

The effect of the independent variables revealed values offering the optimum responses. This is evident from the polynomial Eq. (4) and the Pareto plot (Fig. 3). Using a computer optimization process, we selected the values of 2 g, 1.05 g, and 80 µl for Alg, Chi, and Rom, respectively, as optimum for the formulation of Alg-Chi-Rom. This offers the highest sperm motility of 24,84 µm/s (±4.68). To validate the experimental design, a fresh formulation was prepared at the optimum levels of the independent variables and evaluated for responses. The observed values of sperm motility were 29.25 µm/s (±0.33), which is significantly close to those revealed in the theoretical investigation. Hence, the current model provided satisfactory predictions for Alg-Chi-Rom.

ANN modeling

In the present work, we have found that the amount of Alg, Chi, and Rom could increase the levels of sperm motility. This indicates that sperm motility was well determined in response to the current experimental stage. However, it is still unable to find the global optimal point and extrapolate beyond the experimental range. The ANN method represents a promising modeling technique when applied to control the nonlinear multivariate process [70]. It has been used to investigate the possible interactions of reaction parameters and to optimize the formulation of Alg-Chi-Rom. The best ANN model can be optimally determined from several Box–Behnken design (BBD) data sets employing networks based on the root mean squared errors (RMSE) that were statistically calculated from the actual values and prediction values of each network [71]. In this study, the obtained data using the BBD (Table 2) were further employed to generate an ANN model for optimizing Alg-Chi-Rom. As shown in Fig. 1, the ANN modeling is proposed to consist of three layers: an input layer with three neurons (Alg, Chi, and Rom), a hidden layer with seven neurons, and an output layer containing one

output neuron (sperm motility). The obtained results from experimental trials using an ANN model for sperm motility have been predicted using Eqs. (6–16):

$$Y = 11.855 + 92.766 * H_{1-1} + 314.542 * H_{1-2} - 211.358 * H_{1-3} + 8.482 * H_{1-4} + 153.909 * H_{1-5} - 86.878 * H_{1-6} - 345.465 * H_{1-7} \tag{6}$$

$$H_{2-1} = \mathrm{Tan}H(0.5(0.494 + (0.296 \cdot \mathrm{Alg}) + (0.016 \cdot \mathrm{Chi}) - (0.005 \cdot \mathrm{Rom}))) \tag{7}$$

$$H_{2-2} = 0.064 + (0.529 \cdot \mathrm{Alg}) + (0.898 \cdot \mathrm{Chi}) - (0.021 \cdot \mathrm{Rom}) \tag{8}$$

$$H_{2-3} = \mathrm{Exp}\left(-\left(0.5(0.577 - (0.252 \cdot \mathrm{Alg}) + (1.311 \cdot \mathrm{Chi}) - (0.014 \cdot \mathrm{Rom}))^2\right)\right) \tag{9}$$

$$H_{1-1} = \mathrm{Tan}H\left(0.5\left(-0.365 - \left(0.283 * H_{2-1}\right) + \left(1.204 * H_{2-2}\right) + \left(1.332 * H_{2-3}\right)\right)\right) \tag{10}$$

$$H_{1-2} = \mathrm{Tan}H\left(0.5\left(1.063 + \left(0.283 * H_{2-1}\right) + \left(0.336 * H_{2-2}\right) - \left(0.346 * H_{2-3}\right)\right)\right) \tag{11}$$

$$H_{1-3} = \mathrm{Tan}H\left(0.5\left(-0.728 - \left(2.389 * H_{2-1}\right) + \left(0.362 * H_{2-2}\right) - \left(1.006 * H_{2-3}\right)\right)\right) \tag{12}$$

$$H_{1-4} = -0.120 - \left(0.286 * H_{2-1}\right) + \left(2.358 * H_{2-2}\right) - \left(1.748 * H_{2-3}\right) \tag{13}$$

$$H_{1-5} = 0.721 - \left(0.669 * H_{2-1}\right) - \left(0.549 * H_{2-2}\right) - \left(0.800 * H_{2-3}\right) \tag{14}$$

$$H_{1-6} = 0.957 + \left(0.469 * H_{2-1}\right) - \left(0.645 * H_{2-2}\right) - \left(0.777 * H_{2-3}\right) \tag{15}$$

$$H_{1-7} = \mathrm{Exp}\left(-\left(0.5\left(0.632 - \left(0.358 * H_{2-1}\right) + \left(0.401 * H_{2-2}\right) - \left(0.167 * H_{2-3}\right)\right)^2\right)\right) \tag{16}$$

The artificial neural network's modeling for sperm motility was contrasted with the real data displayed. Table 4 represents the estimation parameters of the obtained ANN model for training and validation data for sperm motility. The R^2 values were used to determine the network system's accuracy at each stage (training and validation). The R^2 value for the sperm motility model was determined to be 0.999 for training and 0.995 for validation. At all phases, it was clear that the neural network worked excellently. As the error rate increased, the network training was halted. Table 4 displays the root mean square error (RMSE) results. The RMSE values for sperm motility were 0.209 and 1.382 for training and validation, respectively. This shows that the neural network performed well at all levels. This parameter also measures the correlation between predicted responses and the target. The association between the output (ANN-predicted sperm motility) and the target (experimental sperm motility) is frequently associated with RMSE values, which have to be less than 3 [72]. As shown in Table 2, the findings show a high degree of closeness between the ANN predictions and the actual experimental outcomes. It also

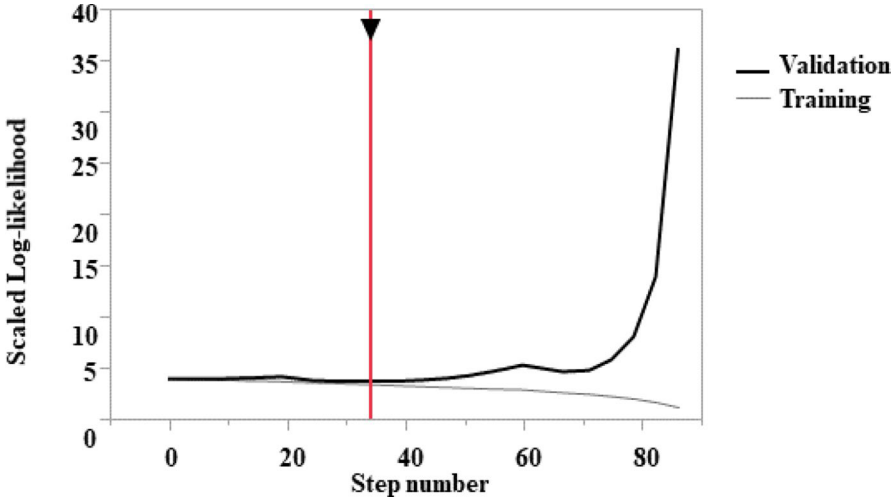

Fig. 4 Path for solution

demonstrates the ANN model's prediction power and validity. For every data set, the log-likelihood function is computed and measures the agreement between theory predictions and experimental measurements. It is a way to measure the goodness of fit for a model. Moreover, it is used to compare performance in modeling [73]. The log-likelihood values for the training and validation sets were −1.561 and 6.969, respectively. This indicates that the log-likelihood obtained at validation was better despite the small size of the data used for validation. This means that the obtained validation is highly significant, which reveals the good validity of the obtained model.

The path for solution indicates which of the obtained models is the most effective (Fig. 4). It represents a great approach for investigating a model's over- or under-fitting. The plot is designed using the scaled negative log probability statistic. The optimal network settings based on the scaled log-likelihood for training and validation were defined. It was obtained at step number 34, where we get the best value for the validation set. After this step, no changes will be observed on the validation set.

Comparison of the predictive capability of RSM and ANN

In general, RSM offers several advantages, such as providing a regression equation for predicting model performance, as well as identifying insignificant main factors, interaction factors, or insignificant quadratic terms in the modeling, thereby simplifying problem complexity compared to ANN [74]. However, RSM is primarily limited to quadratic nonlinear correlations and requires precise range definitions for each element to ensure that the response under examination predictably varies within this defined range [75]. In contrast, ANN can be designed to capture almost any type of nonlinearity, thus surpassing the limitations of RSM [76]. Moreover, this approach does not demand a traditional experimental design for model construction.

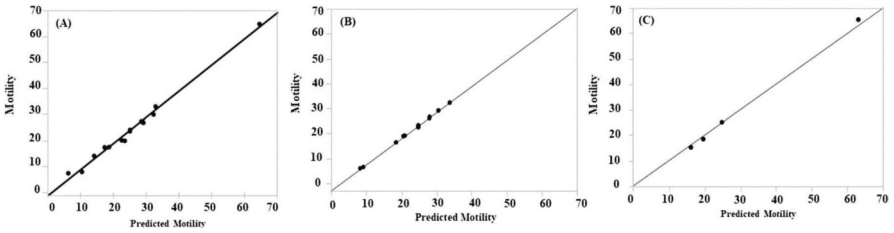

Fig. 5 Observed values against expected values in RSM (**A**) and the different stages of the ANN modeling for sperm motility. (**B**): training; (**C**): validation

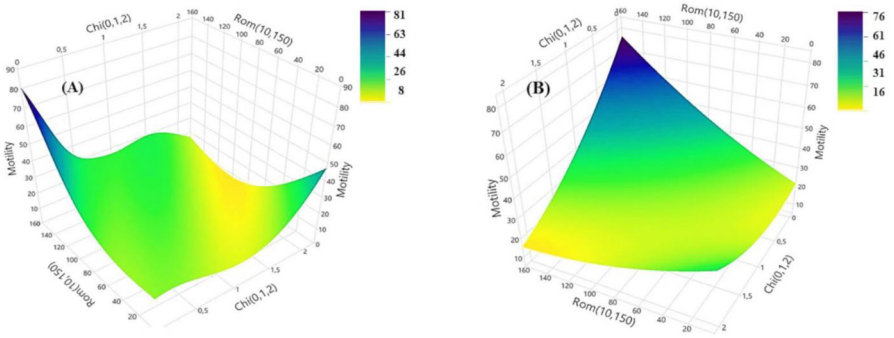

Fig. 6 **A** ANN response surface plots; **B** RSM response surface plots

Therefore, the ANN model exhibits remarkable adaptability, enabling the inclusion of additional experimental variables to create a reliable model [77].

In this study, the optimization and prediction capabilities of the RSM and ANN models were compared based on key performance metrics, including the coefficient of determination (R^2), mean absolute error (MAE), mean absolute percentage error (MAPE), and root mean square error (RMSE).

As shown in Tables 3 and 4, the root mean square error (RMSE) values for sperm motility, obtained from the RSM and ANN models, were 2.165 and 0.209, respectively. This significant difference suggests that the ANN model exhibits better predictive accuracy and validity compared to the RSM model. The coefficient of determination (R^2) values for sperm motility, determined by RSM and ANN, were found to be 0.991 and 0.999, respectively. The mean absolute error (MAE) values for sperm motility, calculated for RSM and ANN, were 1.333 and 1.14, respectively.

Furthermore, Fig. 5 illustrates a scatter plot comparing ANN and RSM predicted sperm motility to the actual sperm motility values. This plot highlights the strong agreement between both models and the experimental data, indicating the accuracy of both approaches. Nevertheless, the ANN model surpasses the RSM model in terms of prediction accuracy.

The contour and surface response plots analyze and forecast the optimal Alg-Chi-Rom formulation (Fig. 6). The interaction effects of experimental factors on

sperm motility generated by ANN were further examined and compared to those observed in RSM interaction plots. The findings indicate that the interaction effects of experimental variables on sperm motility in Alg-Chi-Rom ANN's surface plots are closely similar to those reported in RSM's surface plots. However, ANN modeling's prediction capacity is superior and more accurate than RSM modeling (varying degrees of curvature). These observations complemented those made during the study of the effects of Chi and Rom on sperm motility previously discussed.

Characterization of the optimal Alg-Chi-Rom

High-performance liquid chromatography (HPLC) analysis

Camphor is a crucial component of Algerian rosemary oil. In Fig. 7, the results of camphor identification within the (Alg-Chi-Rom) system are presented. The peak of the camphor standard and the optimal (Alg-Chi-Rom) sample both appear at approximately 5.95 min. Notably, there is no peak observed in the placebo sample within the same time frame. The presence of a peak in the optimal sphere sample at 5.95 min, corresponding to the retention time of camphor, indicates the presence of camphor in the rosemary oil. Additionally, it suggests the formation of complexes between Rom-alginate and chitosan. This is further supported by the absence of peaks in the placebo sample, which lacks oil in its formulation. Consequently, it can be inferred that Rom has been successfully encapsulated through complex formation within the sodium Alg-Chi sphere.

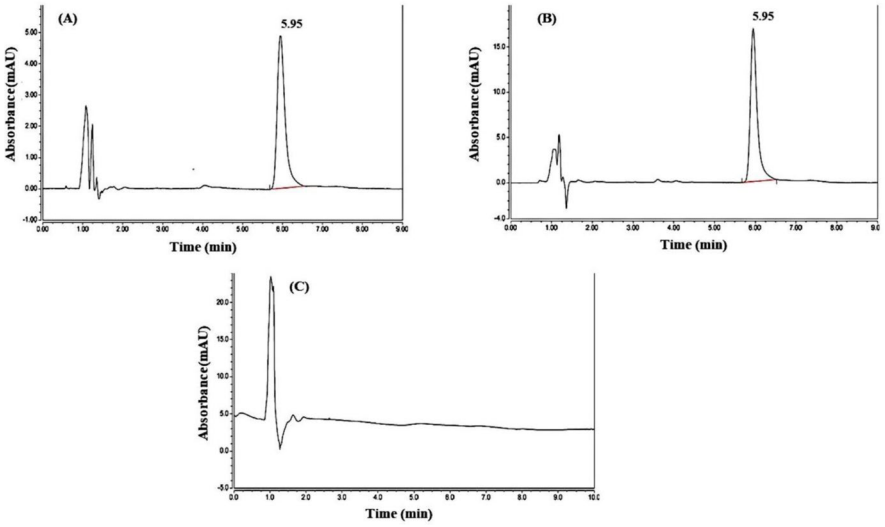

Fig. 7 HPLC chromatograph of **A** Camphor; **B** Rom-Chi-Alg; **C** Placebo

Table 5 The drug entrapment efficiency (DEE) and swelling index at pH (1.2, 6.8, 7.4)

Formulations code	Composition	DEE %	Swelling index at pH		
			1.2	6.8	7.4
F1	Optimum (Rom-Alg-Chi)	85 ± 2.9	50.85 ± 4.5	100 ± 4.1	90 ± 5.1
F2	Rom-Chi	60 ± 4.8	45 ± 4.7	72.22 ± 4.6	80.5 ± 4,9
F3	Rom-Alg	55 ± 3.4	62.5 ± 4.6	83.33 ± 4.5	150 ± 5.3

Each observation is the mean ± S.D ($n = 3$)

Determination of drug entrapment efficiency (DEE)

The results of the drug entrapment efficiency study for the three formulations, namely Optimum (F1), Rom-Chi (F2), and Rom-Alg (F3), are presented in Table 5. The entrapment efficiency is influenced by the presence of chitosan and alginate, indicating that both polymers contribute to increased drug entrapment. Specifically, F1 exhibits the highest drug entrapment efficiency, approximately 85%, whereas F2 shows an entrapment efficiency of around 60%, and F3 demonstrates the lowest drug entrapment efficiency, at 55%. These findings highlight the significant role of chitosan and alginate in enhancing drug entrapment, with the optimal formulation (F1) achieving the highest efficiency.

Drug-excipient interaction study results by Fourier transforms infrared spectroscopy

Chitosan flakes, Na-alginate, and their physical mixture, along with the optimum formulation, have shown characteristic peaks around 3400 cm^{-1} for OH and NH_2

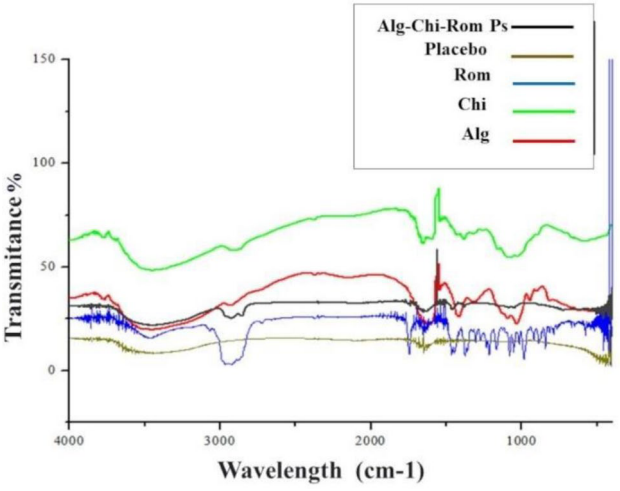

Fig. 8 The FITR spectra

stretching. CH stretching at 2973 cm^{-1} has been seen very significantly in formulation 1 but was not significant in the other formulations (Fig. 8). In sodium alginate, some distinct peaks, such as the carboxyl group, showed strong absorption bands at 1642 cm^{-1} due to carboxyl anions' asymmetric and symmetric stretching vibrations disappearing or becoming weak in the microparticle formulations, which have shown evidence of multi-interactions (hydrogen bonding and electrostatic interaction) among chitosan and alginate molecules, supporting the previous work of Li et al. (2008) [78]. However, all of the FTIR reports have shown OH stretching at 3420 cm^{-1} and OH bending at around 1467 cm^{-1}. Also, there were significant peaks from 1600 to 1500 cm^{-1} due to the presence of the amine group present in chitosan. This observation indicates that there is no significant intermolecular interaction in the physical mixtures or ions.

Swelling index study

The study analyzed the swelling characteristics of the spheres listed in Table 5 by measuring their water absorption at specific time intervals under pH conditions of 1.2, 6.8, and 7.4. At pH 1.2, the spheres from all three formulations exhibited minimal water absorption, which remained consistent regardless of time. The gradual elevation in chitosan concentration within F1, F2, and F3 formulations effectively regulated the swelling of the spheres across all three buffer solutions. The maximum water uptake for all three formulations was seen for 7 h. Up to this point, the spheres function as a matrix for the controlled release of an encapsulated drug, followed by subsequent erosion and disintegration of the spheres. All formulations exhibited a rapid swelling rate, attributable to their high capacity, characterized by macropores within the particles, allowing the spheres to absorb significant amounts of water. The swelling index is comparatively lower in F2 and F3. This could be attributed to the absence of cross-linked functional groups in these formulations, resulting in reduced resistance against the expansion and infiltration of water molecules into their structure [79].

Lipid peroxidation and sperm motility

The lipid peroxidation state was assessed after spontaneous peroxidation. After 48 h of storage, findings presented in Fig. 9 show that MDA levels decreased both in the sperm sample treated with Rom and Alg-Chi-Rom. High levels of MDA are observed in the control group. The ANOVA test showed no significant difference between all treatments.

The objective of incorporating supplements into the sperm dilution solution is to enhance spermatozoa survival and fertilization after chilling for subsequent use in artificial insemination or in vitro fertilization [80]. The impacts of different supplements are evaluated relative to the control (no treatment) and within the same time frame [81, 82]. Kinetic parameters measured with a CASA system revealed the most motility protection (VCL, VSL, and VAP) using the optimal Alg-Chi-Rom formulation (Fig. 10). However, Rom also showed significant motility protection at 0.8 µl ml^{-1} concentration, compared to the control. Rom is a typical lipophilic

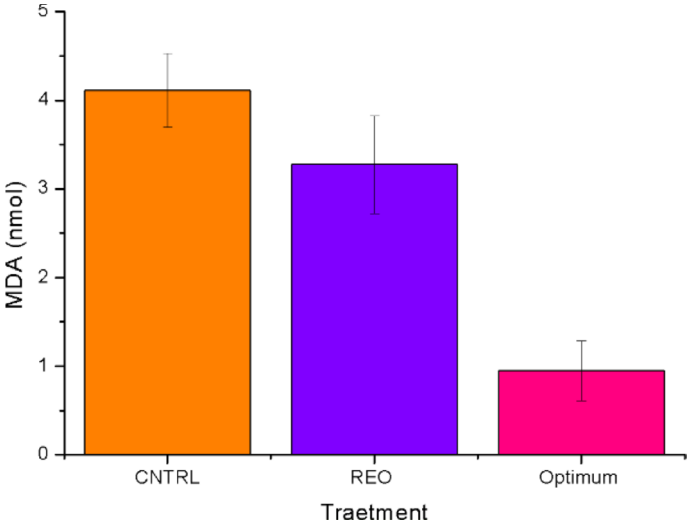

Fig. 9 MDA rate (nmol) after 48 h of 4 °C storage of ram epididymal sperm in the control group (Control) and groups treated with Rom and Alg-Chi-Rom. Different letters indicate significant differences ($P < 0.05$). Values are presented as mean ± SEM

compound, and in a liquid medium such as sperm extenders, the diffusion and dispersion of Rom components are not optimal. Moreover, Rom could be influenced strongly by processing and storage conditions. It could be easily altered due to exposure to direct humidity, light, or oxygen. Furthermore, it has been previously established that using alginate in encapsulation represents an effective method for shielding active compounds of essential oils from environmental factors and enhancing their solubility in aqueous environments, which facilitates the targeted delivery to molecules of interest [83]. The beneficial effect of Rom could be attributed to the wide spectrum of potential biological activities [84], especially those related to its potent antioxidant activity. Polyphenols, molecules different from essential oils, have shown their value in oxidative stress and membrane integrity protection during cryopreservation [40, 85]. In this report, the antioxidant activity is more important in samples treated with Alg-Chi-Rom. The current results showed that these positive effects of Rom are more patented in the presence of Alg-Chi. In our study, the loss of motility is estimated to be between 11 and 31% in samples treated with Ag-Chi-Rom. According to the literature, the quality of spermatozoa after preservation is significantly reduced, with a loss of motility ranging from 40 to 60% [86]. The obtained results show that the Alg-Chi-Rom system is effective as an extender in sperm preservation media.

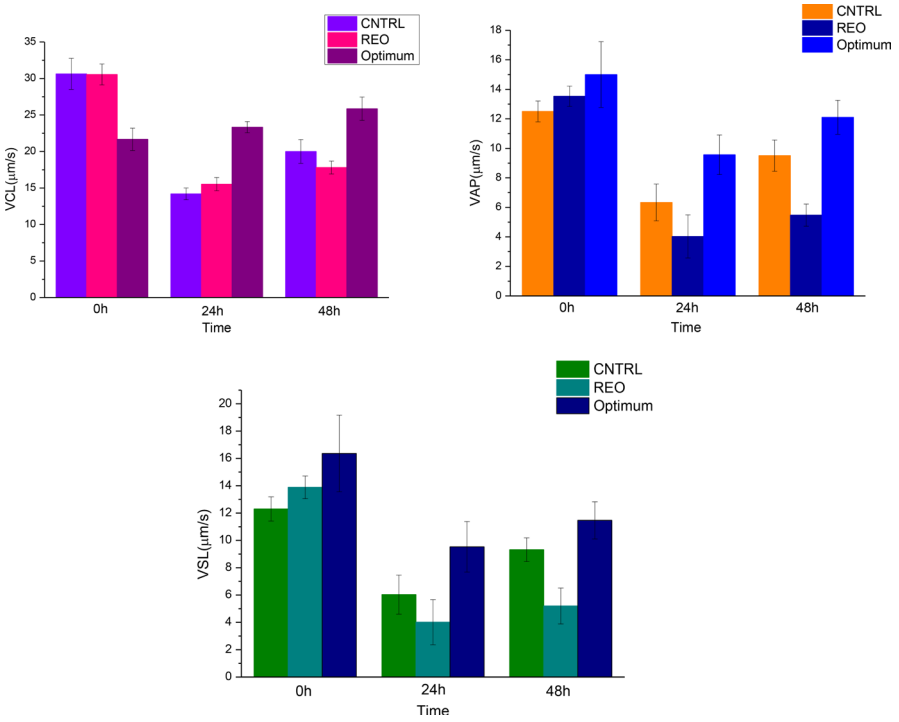

Fig. 10 Mean (±SEM) values for curvilinear velocity (VCL), straight linear velocity (VSL), and average path velocity (VAP) after 0, 24, and 48 h of preservation at 4 °C of bovine epididymal sperm in the control group (Control) and groups treated with Rom and Alg-Chi-Rom. Different letters indicate significant differences ($P < 0.05$)

Conclusion

In this study, we delved into the intricate interactions between polymers, namely Alg, Chi, and Rom, intending to formulate spherical particles. RSM and ANN models proved highly effective in determining the optimal conditions for creating these spherical particles. Notably, ANN outperformed RSM models across all levels, demonstrating a superior correlation between actual test values and predicted values. The Alg/Chi/Rom spherical particles were prepared using a cross-linking method that involved varying concentrations of polymer solutions and Rom. The formulation that exhibited the highest sperm motility (24.84% ± 4.68) comprised 2 g Alg, 1.05 g Chi, and 80 µL of Rom. As confirmed by HPLC and FTIR results, the presence of a camphor peak in the rosemary oil and the Alg-Chi-Rom spherical particles underscored the formation of a complex in the optimal formulation. Furthermore, the Alg-Chi-Rom particles acted as a matrix for the controlled release of the integrated drug. As a result, sphere erosion and disintegration were observed. The optimal formulation displayed the highest antioxidant activity, highlighting its potential to protect against oxidative damage. Finally, utilizing a CASA system, we

assessed the kinetic parameters, VCL, VSL, and VAP. These parameters revealed that the optimal Alg-Chi-Rom particle formulation provided the most effective preservation of sperm motility, particularly after 48 h of storage. This study offers valuable insights into the development of Alg-Chi-Rom particles as a promising approach for various applications. The combination of biopolymers with natural compounds could represent a promising alternative to synthetic polymers and active ingredients commonly used in cell cryopreservation (as supplements in preservation media), as well as in pharmaceutical and nutritional fields.

Acknowledgements The authors gratefully acknowledge the Algerian Ministry of Higher Education and Scientific Research (MESRS), General Direction of Scientific Research and Technological Development (DGRSDT). We also acknowledge Professor YAHIAOUI Idris for supplying us with sodium alginate.

Author contributions All authors listed have made a substantial, direct and intellectual contribution to the work.

Funding No funding was received for the preparation of this manuscript.

Data availability No datasets were generated or analyzed during the current study.

Declarations

Conflict of interest The authors declare that they have no conflict of Interest.

Ethical approval No ethics approval was required.

References

1. Reis SF, Martins VJ, Bastos R et al (2023) Feasibility of Brewer's spent yeast microcapsules as targeted oral carriers. Foods 12:246. https://doi.org/10.3390/foods12020246
2. Bus A, van Hoeck V, Langbeen A et al (2018) Effects of vitrification on the viability of alginate encapsulated isolated bovine pre-antral follicles. J Assist Reprod Genet 35:1187–1199. https://doi.org/10.1007/s10815-018-1208-3
3. Chen R, Wang B, Liu Y et al (2018) A study of cryogenic tissue-engineered liver slices in calcium alginate gel for drug testing. Cryobiology 82:1–7. https://doi.org/10.1016/j.cryobiol.2018.05.002
4. Vanacker J, Amorim CA (2017) Alginate: a versatile biomaterial to encapsulate isolated ovarian follicles. Ann Biomed Eng 45:1633–1649. https://doi.org/10.1007/s10439-017-1816-6
5. Jalayeri M, Pirnia A, Najafabad EP et al (2017) Evaluation of alginate hydrogel cytotoxicity on three-dimensional culture of type A spermatogonial stem cells. Int J Biol Macromol 95:888–894. https://doi.org/10.1016/j.ijbiomac.2016.10.074
6. Pirnia A, Parivar K, Hemadi M, Yaghmaei P, Gholami M (2017) Stemness of spermatogonial stem cells encapsulated in alginate hydrogel during cryopreservation. Andrologia 49(5):e12650. https://doi.org/10.1111/and.12650
7. Taouzinet L, Fatmi S, Khellouf A, Lahiani-Skiba M, Skiba M, Iguer-Ouada M (2022) Drug release, stability and efficiency of vitamin e loaded in liposomes for bovine sperm protection in cryopreservation medium. Cryo Lett 43(1):50–57. https://doi.org/10.54680/fr22110110612
8. Taouzinet L, Fatmi S, Khellouf A, Skiba M, Iguer-ouada M (2020) Alpha tocopherol loaded in liposome: preparation, optimization, characterization and sperm motility protection. Drug Deliv Lett 10(3):228–236. https://doi.org/10.2174/2210303110666200302113209

9. Fatmi S, Taouzinet L, Skiba M, Iguer-Ouada M (2023) Camptothecin: solubility, in-vitro drug release, and effect on human red blood cells and sperm cold preservation. Cryo Lett 44:89–99. https://doi.org/10.54680/fr23210110712
10. Fatmi S, Taouzinet L, Benslimane A et al (2022) Drug release and sperm motility protection studies of vitamin E encapsulated in liposome, cyclodextrin or polyethylene glycol. Mater Today Proceed 53:71–75. https://doi.org/10.1016/j.matpr.2021.12.332
11. Su X, Toublan F, Yin Y, Cadwallader KR (2023) Chapter 22—fats and waxes in microencapsulation of food ingredients. In: Sobel R (ed) Microencapsulation in the food industry (Second Edition). Academic Press, pp 325–342
12. Lee J, Seo HS, Park CG, Shin M (2024) Mucoadhesive and antifouling Janus polysaccharide film for prevention of colorectal cancer recurrence post-surgery. BMEMat. https://doi.org/10.1002/bmm2.12071
13. Cruz Sánchez E, García MT, Gracia I et al (2024) Antibacterial activity assessment of chitosan/alginate lavender essential oil membranes for biomedical applications. Membranes 14:12. https://doi.org/10.3390/membranes14010012
14. Singh N, Anand SK, Sharma A et al (2024) Chitosan/alginate nanogel potentiate berberine uptake and enhance oxidative stress mediated apoptotic cell death in HepG2 cells. Int J Biol Macromol 257:128717. https://doi.org/10.1016/j.ijbiomac.2023.128717
15. Saigl Z, Tifouti O, Alkhanbashi B et al (2023) Chitosan as adsorbent for removal of some organic dyes: a review. Chem Pap 77:2363–2405. https://doi.org/10.1007/s11696-022-02641-y
16. Khalaf EM, Abood NA, Atta RZ et al (2023) Recent progressions in biomedical and pharmaceutical applications of chitosan nanoparticles: a comprehensive review. Int J Biol Macromol 231:123354. https://doi.org/10.1016/j.ijbiomac.2023.123354
17. Liu J, Pu H, Liu S et al (2017) Synthesis, characterization, bioactivity and potential application of phenolic acid grafted chitosan: a review. Carbohydr Polym 174:999–1017. https://doi.org/10.1016/j.carbpol.2017.07.014
18. Hellali DH, Ayachi N (2023) Nanoencapsulation *of Rosmarinus officinalis* essential oil into chitosan crosslinked to tripolyphosphate nanoparticles and alginate/chitosan nanoparticles: formulation, characterization, in vitro release study, and in vivo evaluation. J Drug Deliv Ther 13(11):45–55. https://doi.org/10.22270/jddt.v13i11.6270
19. Martău GA, Mihai M, Vodnar DC (2019) The use of chitosan, alginate, and pectin in the biomedical and food sector—biocompatibility, bioadhesiveness, and biodegradability. Polymers 11(11):1837. https://doi.org/10.3390/polym11111837
20. Jiang M, Althomali RH, Ansari SA et al (2023) Advances in preparation, biomedical, and pharmaceutical applications of chitosan-based gold, silver, and magnetic nanoparticles: a review. Int J Biol Macromol 251:126390. https://doi.org/10.1016/j.ijbiomac.2023.126390
21. Lim AW, Talley NJ, Walker MM et al (2023) Current status and advances in esophageal drug delivery technology: influence of physiological, pathophysiological and pharmaceutical factors. Drug Deliv 30:2219423. https://doi.org/10.1080/10717544.2023.2219423
22. de Moura TCM, Arruda LCP, Cahú TB et al (2023) Carboxymethylchitosan with medium-molecular-weight affects kinectics and acrosome of stallion sperm after freezing/thawing. J Equine Vet Sci 126:104489. https://doi.org/10.1016/j.jevs.2023.104489
23. Safdar R, Omar AA, Arunagiri A et al (2019) Potential of chitosan and its derivatives for controlled drug release applications—a review. J Drug Deliv Sci Technol 49:642–659. https://doi.org/10.1016/j.jddst.2018.10.020
24. Afriani K, Sulaiman S, Maulia G (2023) Synthesis and characterization of hydrogel alginate/poly(N-vinyl-2-pyrrolidone) with double ionic cross-bonded for drug delivery and antibacterial agent. Egypt J Chem. https://doi.org/10.21608/ejchem.2023.209529.7949
25. Adamiak K, Sionkowska A (2023) State of innovation in alginate-based materials. Mar Drugs 21:353. https://doi.org/10.3390/md21060353
26. Sánchez-Hernández E, Santiago-Aliste A, Correa-Guimarães A et al (2024) Carvacrol encapsulation in chitosan-carboxymethylcellulose-alginate nanocarriers for postharvest tomato protection. Int J Mol Sci 25:1104. https://doi.org/10.3390/ijms25021104
27. Afzal S, Maswal M, Dar AA (2018) Rheological behavior of pH responsive composite hydrogels of chitosan and alginate: characterization and its use in encapsulation of citral. Coll Surf B Biointerfaces 169:99–106. https://doi.org/10.1016/j.colsurfb.2018.05.002

28. Natrajan D, Srinivasan S, Sundar K, Ravindran A (2015) Formulation of essential oil-loaded chitosan-alginate nanocapsules. J Food Drug Anal 23:560–568. https://doi.org/10.1016/j.jfda.2015.01.001
29. Meng Y, Qiu C, Li X et al (2024) Polysaccharide-based nano-delivery systems for encapsulation, delivery, and pH-responsive release of bioactive ingredients. Crit Rev Food Sci Nutr 64:187–201. https://doi.org/10.1080/10408398.2022.2105800
30. Moradi M, Hashemian MA, Faramarzi A et al (2024) Therapeutic effect of sodium alginate on bleomycin, etoposide and cisplatin (BEP)-induced reproductive toxicity by inhibiting nitro-oxidative stress, inflammation and apoptosis. Sci Rep 14:1565. https://doi.org/10.1038/s41598-024-52010-w
31. Feng W-J, Mou J, Liao P-P et al (2024) Alginate oligosaccharides exert protective effects on hydrogen peroxide-induced senescence in H_9C_2 cardiomyocytes by regulating the redox state of cells. Food Sci Biotechnol. https://doi.org/10.1007/s10068-024-01534-y
32. Peng Y, Liang S, Meng Q-F et al (2024) Engineered bio-based hydrogels for cancer immunotherapy. Adv Mater 36:e2313188. https://doi.org/10.1002/adma.202313188
33. Kumar P, Pawaria S, Dalal J et al (2019) Sodium alginate potentiates antioxidants, cryoprotection and antibacterial activities of egg yolk extender during semen cryopreservation in buffalo. Anim Reprod Sci 209:106166. https://doi.org/10.1016/j.anireprosci.2019.106166
34. Feyzmanesh S, Halvaei I, Baheiraei N (2022) Alginate effects on human sperm parameters during freezing and thawing: a prospective study. Cell 24:417–423. https://doi.org/10.22074/cellj.2022.8122
35. Chen K, Zhang M, Mujumdar AS, Wang M (2023) Encapsulation of different spice essential oils in quinoa protein isolate-gum Arabic coacervates for improved stability. Carbohydr Polym 300:120250. https://doi.org/10.1016/j.carbpol.2022.120250
36. Olalere OA, Gan C-Y, Taiwo AE et al (2024) Essential oils: sustainable extraction techniques and nutraceuticals perspectives. In: Sarkar T, Pati S (eds) Bioactive extraction and application in food and nutraceutical industries. Springer, US, New York, NY, pp 373–389
37. Oualdi I, Brahmi F, Mokhtari O et al (2021) Rosmarinus officinalis from Morocco, Italy and France: Insight into chemical compositions and biological properties. Mater Today Proceed 45:7706–7710. https://doi.org/10.1016/j.matpr.2021.03.333
38. Huang Y, Heran Xu, Ding M, Li J, Wang Di, Li H, Sun M, Xia F, Bai H, Wang M, Mo M, Shi L (2023) Screening of *Rosemary* essential oils with different phytochemicals for antioxidant capacity, keratinocyte cytotoxicity, and anti-proliferative activity. Molecules 28(2):586. https://doi.org/10.3390/molecules28020586
39. Borges RS, Ortiz BLS, Pereira ACM et al (2019) *Rosmarinus officinalis* essential oil: a review of its phytochemistry, anti-inflammatory activity, and mechanisms of action involved. J Ethnopharmacol 229:29–45. https://doi.org/10.1016/j.jep.2018.09.038
40. Benberkane A, Khellouf A, Benhenia K et al (2019) *Rosmarinus officinalis* essential oil preloaded in β-cyclodextrin: effect on ram spermatozoa motility, membrane integrity and oxidative status during 4 °C storage. Cryo Lett 40:219–225
41. Aberbour A, Touazi L, Benberkane A et al (2023) The effect of in ovo administration of rosemary essential oil on hatchability, relative hatching weight, and embryo mortality rate in Japanese Quail (*Coturnix coturnix japonica*). Animals (Basel) 13:1217. https://doi.org/10.3390/ani13071217
42. Rahmani H, Ghanbariasad A, Meshkibaf MH et al (2024) Chitosan nanoparticles containing α-pinene and *Rosmarinus officinalis L.* essential oil: effects on human melanoma cells' viability and expression of apoptosis-involved genes. Polym Bull 81:2505–2523. https://doi.org/10.1007/s00289-023-04839-w
43. Mehrizad A (2023) Prompt loading and prolonged release of metronidazole by calcium ferrite-carbon nanotubes carrier: optimization and modeling of the process by RSM and ANN. Diam Relat Mater 135:109899. https://doi.org/10.1016/j.diamond.2023.109899
44. Zahran HA, Catalkaya G, Yenipazar H et al (2023) Determination of the optimum conditions for emulsification and encapsulation of echium oil by response surface methodology. ACS Omega 8:28249–28257. https://doi.org/10.1021/acsomega.3c01779
45. Khezerlou S, Babazadeh M, Mehrizad A et al (2021) Preparation of hydroxyapatite-calcium ferrite composite for application in loading and sustainable release of amoxicillin: optimization and modeling of the process by response surface methodology and artificial neural network. Ceram Int 47:24287–24295. https://doi.org/10.1016/j.ceramint.2021.05.140

46. Mehrizad A (2017) Adsorption studies of some phenol derivatives onto Ag-cuttlebone nanobiocomposite: modeling of process by response surface methodology. Res Chem Intermed 43:4295–4310. https://doi.org/10.1007/s11164-017-2874-y
47. Fattahi M, Kazemeini M, Khorasheh F, Rashidi AM (2013) Vanadium pentoxide catalyst over carbon-based nanomaterials for the oxidative dehydrogenation of propane. Ind Eng Chem Res 52:16128–16141. https://doi.org/10.1021/ie4007358
48. Safdar R, Thanabalan M (2023) Preparation of chitosan-tripolyphosphate formulated insulin microparticles, their characterization, ANN prediction, and release kinetics. J Pharm Innov 18:1047–1064. https://doi.org/10.1007/s12247-023-09707-8
49. Loganathan V, Vijayan L, Balakrishnaraja R (2023) Optimization of spray drying process parameters to enhance the yield of bioactive substances from *Pithecellobium dulce* leaves and its activity: modelling comparision using response surface methodology and artificial neural network
50. Moeinzadeh A, Ashtari B, Garcia H et al (2023) The effect of chitosan/alginate/graphene oxide nanocomposites on proliferation of mouse spermatogonial stem cells. J Funct Biomater 14:556. https://doi.org/10.3390/jfb14120556
51. Hazra M, Dasgupta Mandal D, Mandal T et al (2015) Designing polymeric microparticulate drug delivery system for hydrophobic drug quercetin. Saudi Pharm J 23:429–436. https://doi.org/10.1016/j.jsps.2015.01.007
52. Khaled E, Abo El-Ela FI, El-Nesr KA et al (2020) An herbal nanohybrid formula of epigallocatechin gallate-chitosan-alginate efficiently restrict the sexual dysfunction adverse effect of β-adrenergic antagonist drug: propranolol. J Biomed Nanotechnol 16:505–519. https://doi.org/10.1166/jbn.2020.2915
53. Zhang Y, Wei W, Lv P et al (2011) Preparation and evaluation of alginate-chitosan microspheres for oral delivery of insulin. Eur J Pharm Biopharm 77:11–19. https://doi.org/10.1016/j.ejpb.2010.09.016
54. Patra T, Gupta MK (2020) Evaluation of sodium alginate for encapsulation-vitrification of testicular Leydig cells. Int J Biol Macromol 153:128–137. https://doi.org/10.1016/j.ijbiomac.2020.02.233
55. Guinebretière S, Briançon S, Fessi H et al (2002) Nanocapsules of biodegradable polymers: preparation and characterization by direct high resolution electron microscopy. Mater Sci Eng C 21:137–142. https://doi.org/10.1016/S0928-4931(02)00073-5
56. Kaveh A, Eskandari A, Movasat M (2023) Buckling resistance prediction of high-strength steel columns using metaheuristic-trained artificial neural networks. Structures 56:104853. https://doi.org/10.1016/j.istruc.2023.07.043
57. Piotrowski AP, Napiorkowski JJ (2013) A comparison of methods to avoid overfitting in neural networks training in the case of catchment runoff modelling. J Hydrol 476:97–111. https://doi.org/10.1016/j.jhydrol.2012.10.019
58. Martinez-Pastor F, Garcia-Macias V, Alvarez M et al (2006) Comparison of two methods for obtaining spermatozoa from the cauda epididymis of Iberian red deer. Theriogenology 65:471–485. https://doi.org/10.1016/j.theriogenology.2005.05.045
59. Benhenia K, Lamara A, Fatmi S, Iguer-Ouada M (2016) Effect of cyclodextrins, cholesterol and vitamin E and their complexation on cryopreserved epididymal ram semen. Small Rumin Res 141:29–35. https://doi.org/10.1016/j.smallrumres.2016.06.009
60. Buege JA, Aust SD (1978) Microsomal lipid peroxidation. Methods Enzymol 52:302–310. https://doi.org/10.1016/s0076-6879(78)52032-6
61. Kribeche A, Ben Hamiche N, Ladjouze B, Arbaoui S (2023) Optimization of coagulation-flocculation process with dehulled and unhulled *Moringa oleifera* cake powder by 25 full factorial design and artificial neural networks: effect on dam water quality. Urban Water J 20:910–924. https://doi.org/10.1080/1573062X.2023.2217656
62. Myers RH, Montgomery DC, Anderson-Cook CM (2011) Response Surface Methodology: Process and Product Optimization Using Designed Experiments. John Wiley & Sons
63. Qian J, Wang X, Chen Y et al (2023) The correlation of molecule weight of chitosan oligomers with the corresponding viscosity and antibacterial activity. Carbohydr Res 530:108860. https://doi.org/10.1016/j.carres.2023.108860
64. Xu Y, Sun H, Lv J et al (2023) Effects of polysaccharide thickening agent on the preparation of walnut oil oleogels based on methylcellulose: characterization and delivery of curcumin. Int J Biol Macromol 232:123291. https://doi.org/10.1016/j.ijbiomac.2023.123291

65. Ebrahim SA, Othman HA, Mosaad MM, Hassabo AG (2023) Eco-friendly natural thickener (pectin) extracted from fruit peels for valuable utilization in textile printing as a thickening agent. Text Usages Tech 3:26–49. https://doi.org/10.3390/textiles3010003
66. Abourehab MAS, Rajendran RR, Singh A et al (2022) Alginate as a promising biopolymer in drug delivery and wound healing: a review of the state-of-the-art. Int J Mol Sci 23:9035. https://doi.org/10.3390/ijms23169035
67. Frent OD, Vicas LG, Duteanu N et al (2022) Sodium alginate-natural microencapsulation material of polymeric microparticles. Int J Mol Sci 23:12108. https://doi.org/10.3390/ijms232012108
68. Abd El-Hack ME, El-Saadony MT, Shafi ME et al (2020) Antimicrobial and antioxidant properties of chitosan and its derivatives and their applications: a review. Int J Biol Macromol 164:2726–2744. https://doi.org/10.1016/j.ijbiomac.2020.08.153
69. Haaland PD (2020) Experimental design in biotechnology, 1st edn. CRC Press
70. Urrea C, Garcia-Garcia Y (2023) Design and performance analysis of level control strategies in a nonlinear spherical tank. Processes 11:720. https://doi.org/10.3390/pr11030720
71. Xue Z, Fu J, Fu Q et al (2023) Modeling and optimizing the performance of green forage maize harvester header using a combined response surface methodology-artificial neural network approach. Collect FAO Agric 13:1890. https://doi.org/10.3390/agriculture13101890
72. Ejimofor MI, Ezemagu IG, Menkiti MC (2021) RSM and ANN-GA modeling of colloidal particles removal from paint wastewater via coagulation method using modified *Aguleri montmorillonite* clay. Curr Res Green Sustain Chem 4:100164. https://doi.org/10.1016/j.crgsc.2021.100164
73. Hou T-J, Gao J, Hobbs TJ et al (2021) New CTEQ global analysis of quantum chromodynamics with high-precision data from the LHC. Phys Rev D 103:014013. https://doi.org/10.1103/PhysRevD.103.014013
74. Li H, Zhang Z, Liu Z (2017) Application of artificial neural networks for catalysis: a review. Catalysts 7:306. https://doi.org/10.3390/catal7100306
75. de Oliveira LG, de Paiva AP, Balestrassi PP et al (2019) Response surface methodology for advanced manufacturing technology optimization: theoretical fundamentals, practical guidelines, and survey literature review. Int J Adv Manuf Technol 104:1785–1837. https://doi.org/10.1007/s00170-019-03809-9
76. Onu CE, Nwabanne JT, Ohale PE, Asadu CO (2021) Comparative analysis of RSM, ANN and ANFIS and the mechanistic modeling in eriochrome black-T dye adsorption using modified clay. S Afr J Chem Eng 36:24–42. https://doi.org/10.1016/j.sajce.2020.12.003
77. Huang S-M, Kuo C-H, Chen C-A et al (2017) RSM and ANN modeling-based optimization approach for the development of ultrasound-assisted liposome encapsulation of piceid. Ultrason Sonochem 36:112–122. https://doi.org/10.1016/j.ultsonch.2016.11.016
78. Li P, Dai Y-N, Zhang J-P et al (2008) Chitosan-alginate nanoparticles as a novel drug delivery system for nifedipine. Int J Biomed Sci 4:221–228
79. Hamedi H, Moradi S, Tonelli AE, Hudson SM (2019) Preparation and characterization of chitosan-alginate polyelectrolyte complexes loaded with antibacterial thyme oil nanoemulsions. NATO Adv Sci Inst Ser E Appl Sci 9:3933. https://doi.org/10.3390/app9183933
80. Taouzinet L, Fatmi S, Lahiani-Skiba M et al (2021) Encapsulation nanotechnology in sperm cryopreservation: systems preparation methods and antioxidants enhanced delivery. Cryo Lett 42:1–12
81. Uhlmannsiek L, Shen H, Eylers H et al (2024) Preserving frozen stallion sperm on dry ice using polymers that modulate ice crystalization kinetics. Cryobiology 114:104852. https://doi.org/10.1016/j.cryobiol.2024.104852
82. Maulida S, Eriani K, Fadli N et al (2024) Effect of type and concentration of antioxidant on sperm motility, viability, and DNA integrity of climbing perch *Anabas testudineus* Bloch, 1792 (Pisces: Anabantidae) post-cryopreservation. Cryobiology 114:104851. https://doi.org/10.1016/j.cryobiol.2024.104851
83. Yang Z, Li M, Zhai X et al (2022) Development and characterization of sodium alginate/tea tree essential oil nanoemulsion active film containing TiO_2 nanoparticles for banana packaging. Int J Biol Macromol 213:145–154. https://doi.org/10.1016/j.ijbiomac.2022.05.164
84. Angourani HR, Heydari M, Yousefi AR et al (2022) Nanoparticles based-plant protein containing *Rosmarinus officinalis* essential oil; fabrication, characterization, and evaluation. NATO Adv Sci Inst Ser E Appl Sci 12:9968. https://doi.org/10.3390/app12199968

85. Touazi L, Aberkane B, Bellik Y, Moula N, Iguer-Ouada M (2018) Effect of the essential oil of *Rosmarinus officinalis* (L.) on rooster sperm motility during 4 °C short-term storage. Veterinary World 11(5):590–597. https://doi.org/10.14202/vetworld.2018.590-597
86. Kunkitti P, Chatdarong K, Suwimonteerabutr J et al (2017) Osmotic tolerance of feline epididymal spermatozoa. Anim Reprod Sci 185:148–153. https://doi.org/10.1016/j.anireprosci.2017.08.014

Authors and Affiliations

Lamia Taouzinet[1] · Sofiane Fatmi[2,3,4] · Amina Kribeche[5,6] · Mohamed Skiba[4] · Mokrane Iguer-Ouada[2]

✉ Lamia Taouzinet
lamia.taouzinet@crtaa.univ-bejaia.dz; lamia.taouzinet@crtaa.dz

[1] Centre de Recherche en Technologies Agro-Alimentaires, Route de Targa Ouzemmour, Campus Universitaire, 06000 Bejaia, Algeria

[2] Associated Laboratory in Marine Ecosystems and Aquaculture, Faculty of Nature and Life Sciences, Université de Bejaia, 06000 Bejaia, Algeria

[3] Technology Pharmaceutical Laboratory, Department of Process Engineering, Faculty of Technology, Université de Bejaia, 06000 Bejaia, Algeria

[4] Technology Pharmaceutical and Biopharmaceutics Laboratory, UFR Medicine and Pharmacy, Rouen University, 22 Blvd. Gambetta, 76183 Rouen, France

[5] Department of Food Sciences, Faculty of Natural Sciences and Life, Mouloud Mammeri University, 15000 Tizi-Ouzou, Algeria

[6] Laboratoire de Biomathématique, Biochimie, Biophysique Et Scientométrie, Faculté Des Sciences de La Nature Et de La Vie, Université de Bejaia, 06000 Bejaia, Algeria